Study of the Electrode/Electrolyte Interface on Cycling of a Conversion Type Electrode Material in Li Batteries

ARTICLE *in* THE JOURNAL OF PHYSICAL CHEMISTRY C · AUGUST 2013

Impact Factor: 4.77 · DOI: 10.1021/jp402973h

11 AUTHORS, INCLUDING:

Cyril Marino
Technische Universität München
20 PUBLICATIONS **283** CITATIONS
SEE PROFILE

Nicolas Dupré
French National Centre for Scientific Research
54 PUBLICATIONS **1,264** CITATIONS
SEE PROFILE

Bernard Lestriez
Institut des Materiaux Jean Rouxel
124 PUBLICATIONS **1,538** CITATIONS
SEE PROFILE

Herve Martinez
Université de Pau et des Pays de l'Adour
120 PUBLICATIONS **1,590** CITATIONS
SEE PROFILE

THE JOURNAL OF PHYSICAL CHEMISTRY C

Article

pubs.acs.org/JPCC

Study of the Electrode/Electrolyte Interface on Cycling of a Conversion Type Electrode Material in Li Batteries.

C. Marino,[†] A. Darwiche,[†] N. Dupré,[‡] H. A. Wilhelm,[‡] B. Lestriez,[‡] H. Martinez,[§] R. Dedryvère,[§] W. Zhang,[§,⊥] F. Ghamouss,[⊥] D. Lemordant,[⊥] and L. Monconduit*[,†]

[†]Institut Charles Gerhardt Montpellier-UMR 5253 CNRS, ALISTORE European Research Institute (3104 CNRS), Université Montpellier 2, 34095, Montpellier, France

[‡]Institut des Matériaux Jean Rouxel (IMN), CNRS UMR 6502, Université de Nantes, 44322, Nantes Cedex 3, France

[§]IPREM-ECP CNRS UMR 5254, Helioparc Pau-Pyrénées, 2 Av du Pdt Angot, 64053 Pau Cedex, France

[⊥]Université F. Rabelais, Lab. PCM2E, Faculté des Sciences et Techniques, Parc de Grandmont, 37200 Tours, France

ABSTRACT: Previous work demonstrated that TiSnSb is a promising negative electrode material with high electrochemical performance due to the benefit of conversion type reaction vs Li. At low potentials, the volumetric change upon cycling entails electrolyte degradation which remains the main factor limiting the cycling life of TiSnSb based electrodes. To further improve the understanding of the formation of a solid electrolyte interphase (SEI) in the presence of alkyl carbonate based electrolytes and of its evolution upon cycling, powerful surface characterization techniques are combined for studying the electrode/electrolyte interface of TiSnSb composite electrodes. Electrochemical impedance spectroscopy is used for monitoring in situ the resistivity of the SEI, while XPS and solid state NMR spectroscopy can provide useful information on the SEI chemical composition and its evolution during cycling.

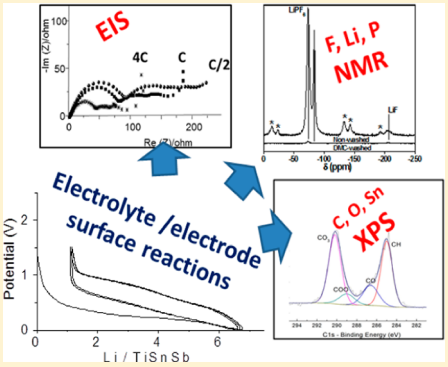

1. INTRODUCTION

Li-ion batteries are nowadays considered as the technology of choice for electrical energy storage in isolated sites and for portable equipment. However, state-of-the-art Li-ion technologies are just emerging in the field of transportation. Among all types of electrode materials, the limitation in terms of energy density of the Li-ion technology is mainly due to both weak capacities and limited electrodes cycling life. In this context, a technological breakthrough is needed to reach an energy density greater than 500 W h/kg. Conversion materials provide a real technologic breakthrough with their strong gravimetric and volumetric energy densities. This class of materials offers the exchange of up to nine Li per transition metal in pnictides (P, Sb) compared to one or two Li per transition metal M for the classical insertion reactions. During the conversion reaction, the M_xX_y starting material is transformed into a mixture consisting of metallic nanosized particles embedded into a Li_nX matrix, as follows:[1,2]

$$M_xX_y + nye^- + nyLi^+ \leftrightarrows xM^0 + yLi_nX,$$

$$\text{with M = Fe, Ni, Co...; X = S, P, Sb...}$$

Due to kinetic limitations and parasitic reactions, the cycle life of these electrodes is however still too short to be suitable for practical applications. Electrolyte reduction has been identified as one of the main side reactions limiting the longevity of M_xX_y based batteries, but the mechanisms leading to its decomposition remain, at the moment, totally unknown and unexplored. The properties of the SEI layer (solid electrolyte interface), which is fairly often formed when an electrolyte is reduced at the electrode surface, control the kinetics of electrochemical reactions occurring at the electrode/electrolyte interface and, hence, the longevity of the battery. Moreover, the SEI formation leads to an irreversible capacity on the first cycle which can be detrimental to the battery performances.

Previous work demonstrated that TiSnSb can reversibly take up more than five lithium per formula unit leading to reversible capacities of 540 mA h/g or 4070 mA h/cm^3 at 2*C* rate.[3] From XRD in situ operando studies and ^{119}Sn Mössbauer spectroscopy, an electrochemical equation was proposed for Li insertion (discharge):

$$TiSnSb + 6.5Li \rightarrow Ti + Li_3Sb + 0.5Li_7Sn_2$$

On subsequent charges the presence of a ternary alloy close to TiSnSb is the most credible. The TiSnSb powder shows very poor electrochemical performances vs Li; cycling abilities are highly improved when this powder is formulated with carboxymethyl cellulose binder and carbon nanofibres.[4] However, electrolyte reduction and volumetric change on cycling remain the main factors limiting the cycling life of the TiSnSb electrode. Moreover, due to the conversion reaction, the morphology of the fresh electrode material is significantly

Received: March 26, 2013
Revised: August 27, 2013
Published: August 27, 2013

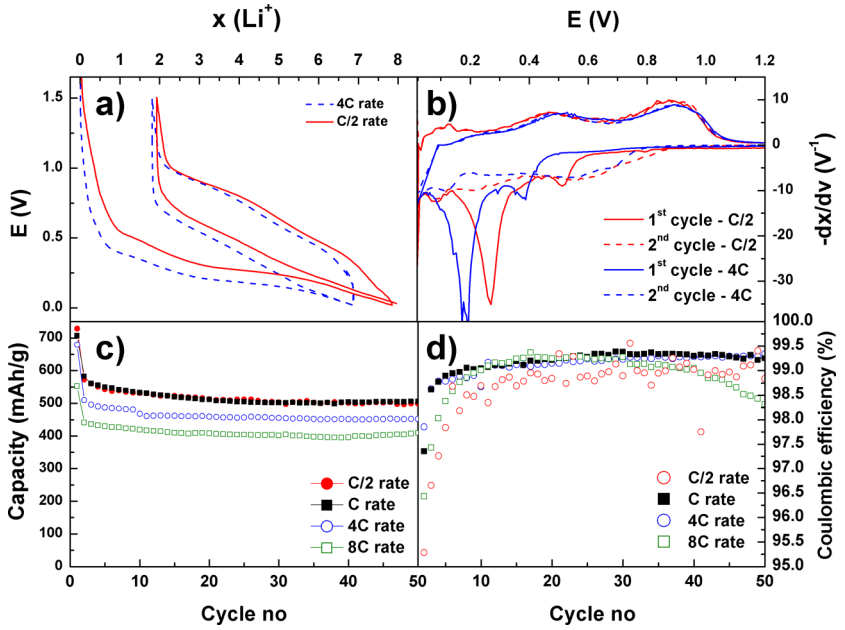

Figure 1. (a) Galvanostatic curve of TiSnSb electrode cycled at C/5 rate between 0.02 and 1.5 V, (b) corresponding derivative curve, (c) capacity retention, and (d) Coulombic efficiencies at various cycling rates.

modified at the first cycle which undoubtedly enhances the electrolyte reduction.[5]

To better understand alkyl carbonate based electrolyte degradation and SEI modification upon cycling, powerful surface characterization techniques were combined for studying the TiSnSb composite electrode/electrolyte interface. Electrochemical impedance spectroscopy (EIS) allows monitoring directly the electrical characteristics of the interfaces, while XPS and MAS NMR spectroscopies[6−8] are designed to provide useful information on the chemical composition of the SEI layer and its evolution during cycling.

2. EXPERIMENTAL DETAILS

Electrochemical Tests. To prepare electrodes, carboxymethyl cellulose (CMC) (DS = 0.7, M_w = 250 000, Aldrich) was used as binder with two conductive additives: (i) vapor grown carbon fibers VGCF (diameter 100−200 nm and length 10−20 μm, SHOWA DENKO) and (ii) carbon black (CB) Y50A (BET primary particle size 20−60 nm, primary aggregate size 100 nm, 70 $m^2 \cdot g^{-1}$, DBP oil absorption 640 mL/100 g, SN2A). TiSnSb powder, CMC, and additives were ground manually in a mortar with a 70/12/9/9% weight ratio (TiSnSb/CMC/Y50A/VGCF). The mixture was then introduced along with deionized water into a silicon nitride vial containing three 9.5 mm diameter silicon nitride balls. A Fritsch Pulverisette 7 was used to mill the mixture at 500 rpm for 1 h. The slurry was tape cast onto a 22 μm thick copper foil at 150 μm thickness. The electrode is named hereafter TSS2. Finally, the obtained electrodes were dried for 12 h at room temperature and then 1 h at 100 °C under vacuum. Swagelok cells were assembled in a glovebox using the composite electrode as positive electrode, a porous glass-fiber paper (WHATMAN) as separator, and metallic lithium as negative electrode. $LiPF_6$ (1 M) dissolved in ethylene carbonate−propylene carbonate−dimethyl carbonate 1:1:3 (v:v:v) with 1% vol of vinylene carbonate (VC) was used as the electrolyte. Cells were cycled at 20 °C using a VMP system (Bio-Logic S.A.) in galvanostatic mode from 0 to 1.5 V vs Li^+/Li. The electrochemical tests were conducted at *C*/*n* (one Li in *n* hours). TSS2 electrodes have been cycled in the alkyl carbonate based electrolyte at *C*/2 or 4*C* rate.

X-ray Photoelectron Spectroscopy. XPS measurements were carried out with a Thermo Scientific K-Alpha X-ray photoelectron spectrometer, using a focused monochromatized Al Kα radiation ($h\nu$ = 1486.6 eV). The XPS spectrometer was directly connected through a glovebox under argon atmosphere, in order to avoid moisture/air exposure of the samples. For the Ag $3d_{5/2}$ line the full width at half-maximum (fwhm) was 0.50 eV under the recording conditions. The X-ray spot size was 400 μm. Peaks were recorded with a constant pass energy of 20 eV. The pressure in the analysis chamber was less than 2×10^{-7} Pa. Short acquisition time spectra were recorded at the beginning and at the end of each experiment to check that the samples did not suffer from degradation during the measurements. The binding energy scale was calibrated from the hydrocarbon contamination using the C 1s peak at 285.0 eV. Core peaks were analyzed using a nonlinear Shirley-type background.[9] The peak positions and areas were optimized by a weighted least-squares fitting method using 70% Gaussian, 30% Lorentzian line shapes. Quantification was performed on the basis of Scofield's relative sensitivity factors.[10]

Electrochemical Impedance Spectroscopy (EIS). Two electrodes coin half-cells, with a lithium foil as counter electrode, were assembled in an argon-filled glovebox. Microporous Celgard membrane and Whatman paper filter filled with the electrolyte solution was used as separator. Galvanostatic charge−discharge, cyclic voltammetry, and electrochemical impedance experiments were performed using a multichannel galvanostat−potentiostat (VMP-Bio-Logic S.A.) piloted by an EC Lab V10.20 interface. Impedance measurements were conducted first at the OCV potential and then at different states of charge during lithiation of the electrode material. The state of charge of the electrode was controlled galvanostatically at different rates of charge/discharge: *C*/2, *C*, and 4*C*. The impedance of the cell was measured in the potentiostatic mode (PEIS) in the frequency range 20−1 MHz with an ac amplitude of 10 mV. Cyclic voltammetry was conducted at a scan rate of

dx.doi.org/10.1021/jp402973h | J. Phys. Chem. C 2013, 117, 19302−19313

25 $\mu V \cdot s^{-1}$ from the OCV to 20 mV vs Li^+/Li and then to a set potential of 1.6 V vs Li/Li^+.

Nuclear Magnetic Resonance (NMR). ^7Li MAS NMR experiments were carried out at room temperature on a Bruker Avance-200 spectrometer (B_0 = 4.7 T, Larmor frequency $\nu_0(^7Li)$ = 77.78 MHz). MAS spectra were obtained by using a Bruker MAS probe with a cylindrical 2.5 mm o.d. zirconia rotor. Spinning frequencies up to 29 kHz were utilized. ^7Li NMR spectra were acquired using a Hahn echo sequence with a $\pi/2$ pulse of 3 μs and a recycle time of 30 s in order to avoid signal saturation and to ensure the complete detection of the ^7Li signals. The isotropic shifts, reported in parts per million, are relative to an external 1 M solution of LiCl in water set at 0 ppm. ^{19}F NMR spectra were acquired at room temperature on a Bruker Avance-500 spectrometer (B_0 = 11.8 T, Larmor frequency $\nu_0(^{19}F)$ = 470 MHz), using a Hahn echo sequence with a $\pi/2$ pulse of 3.6 μs and a recycle time of 30s. ^{31}P NMR spectra were acquired at room temperature on a Bruker Avance-500 spectrometer (B_0 = 11.8 T, Larmor frequency $\nu_0(^{31}P)$ = 202 MHz), using a single pulse sequence with a $\pi/2$ pulse of 4 μs and a recycle time of 30 s. All spectra displayed in this work were normalized taking into account the number of scans, the receiver gain, and the mass of sample. ^7Li and ^{19}F integrated intensities were determined by using spectral simulation (Dmfit software[11]). All samples were washed three times in the DMC right after disassembling the electrochemical cells and prior to ex situ analyses.

3. RESULTS AND DISCUSSION

3.1. Electrochemical Measurements. Figure 1 and Table 1 show the electrochemical behavior of a TiSnSb composite film prepared as described in the experimental part and cycled at C/2 or 4C rate, i.e., the capacity lost after the first cycle, the specific capacity, and polarization voltage (voltage difference between charge and discharge) for the 1st, 2nd, 10th, 20th, and 50th cycles.

Table 1. Electrochemical Behavior of TiSnSb Composite Electrode Measured at C/2 and 4C Rates

		cycle				
cycle number	rate	1st	2nd	10th	20th	50th
charge capacity (mA h g^{-1})	C/2	548 (irr. 24%)	545	524	506	493
	4C	471 (irr. 26%)	459	422	415	409
CE[a] (%)	C/2	75.2	95.3	98.7	98.8	98.8
	4C	73.7	97.9	98.5	99.1	99.3
voltage polarization (V)	C/2	0.318	0.323	0.324	0.335	0.33
	4C	0.362	0.369	0.374	0.405	0.387

[a]Coulombic efficiencies.

Like in all conversion type materials, TiSnSb undergoes a specific low voltage discharge and a large irreversibility capacity at the first cycle (Figure 1a, b): 24 and 26% for respectively C/2 and 4C rates. Figure 1c, d displays the capacity retention and the Coulombic efficiencies for rates ranging from C/2 to 8C. As expected, at high rates (4C and 8C) the capacity is decreased, while at slower rates (C and C/2), a capacity close to the theoretical value (580 mA h g^{-1}) is measured at the first cycle. On the other hand, starting with the second cycle the Coulombic efficiency is higher at high rate (4C) than lower rates (C/2). Moreover, although the capacity is slightly smaller at 4C, the capacity is perfectly maintained at high rates. It is however noteworthy that the global shape of the galvanostatic curve is the same, suggesting that electrochemical processes are unmodified by the choice of the cycling rate. Differences in polarization voltage and Coulombic efficiencies could be attributed to the SEI chemical or electrical properties.

In order to investigate the SEI physicochemical properties in the presence of the alkyl carbonate based electrolytes and follow its evolution upon cycling, an in-depth characterization of species formed at the TiSnSb electrode/electrolyte interface has been investigated by combining EIS, MAS NMR, and XPS experiments.

3.2. Study of SEI Layer during the first Electrochemical Cycles Cyclic Voltammetry (CV). CV analysis was performed at the first cycle, and results are reported in Figure 2.

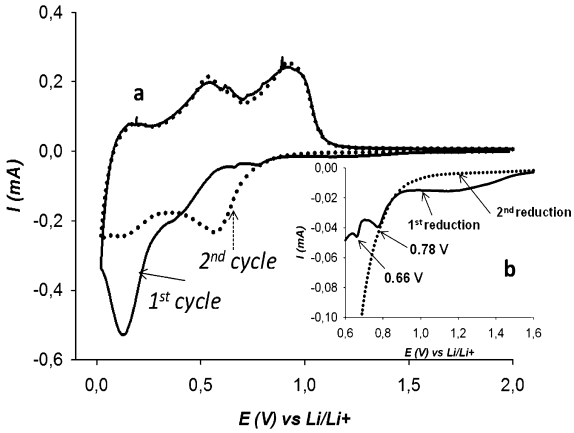

Figure 2. Cyclic voltammograms of TiSnSb electrode at 0.025 $mV \cdot s^{-1}$ between 0.02 and 1.5 V for the first two discharges.

The inset of Figure 2 focuses on the electrochemical reduction of the organic electrolyte in the 0.6−1.6 V potential range.[12,13] In these limits, three peaks are identified at respectively 1.15, 0.78, and 0.66 V. The first peak could be assigned to the reduction of vinylene carbonate (VC) and the subsequent formation of the SEI as this peak does not appear at the second scan. Radical polymerization of VC is well-known and leads to the formation of polyalkyl carbonate species like polymeric chains containing $-OCO_2Li$ groups on the electrode surface.[14] Reduction of the other alkyl carbonate solvents is expected to occur at a slightly lower potential leading to the formation of $ROCO_2Li$, $(CH_2OCO_2Li)_2$, polycarbonate, and byproducts such as Li_2CO_3.[15] The second and the third well-defined peaks at 0.78 and 0.66 V could be attributed to the initial reduction of Sn, Ti, and Sb oxides at the surface of the electrode since these peaks are always visible even when the electrolyte is changed in nature and composition. At the second scan the peak at 1.15 V fully disappears indicating that the formed SEI layer passivates efficiently the electrode surface.

Electrochemical Impedance Spectroscopy (EIS). EIS measurements were carried out on Li/TiSnSb coin cells after the first charge in order to investigate the modifications occurring at the electrode/electrolyte interfaces during cycling. In order to decouple the response of the two electrodes, a Li/Li symmetric cell was used to determine the contribution of the Li foil to the global impedance spectra. As shown in Figure 3a, before cell polarization, the Li/Li symmetric cell displays two depressed semicircles corresponding to the charge transfer resistance/double layer capacitance and the surface film

dx.doi.org/10.1021/jp402973h | J. Phys. Chem. C 2013, 117, 19302−19313

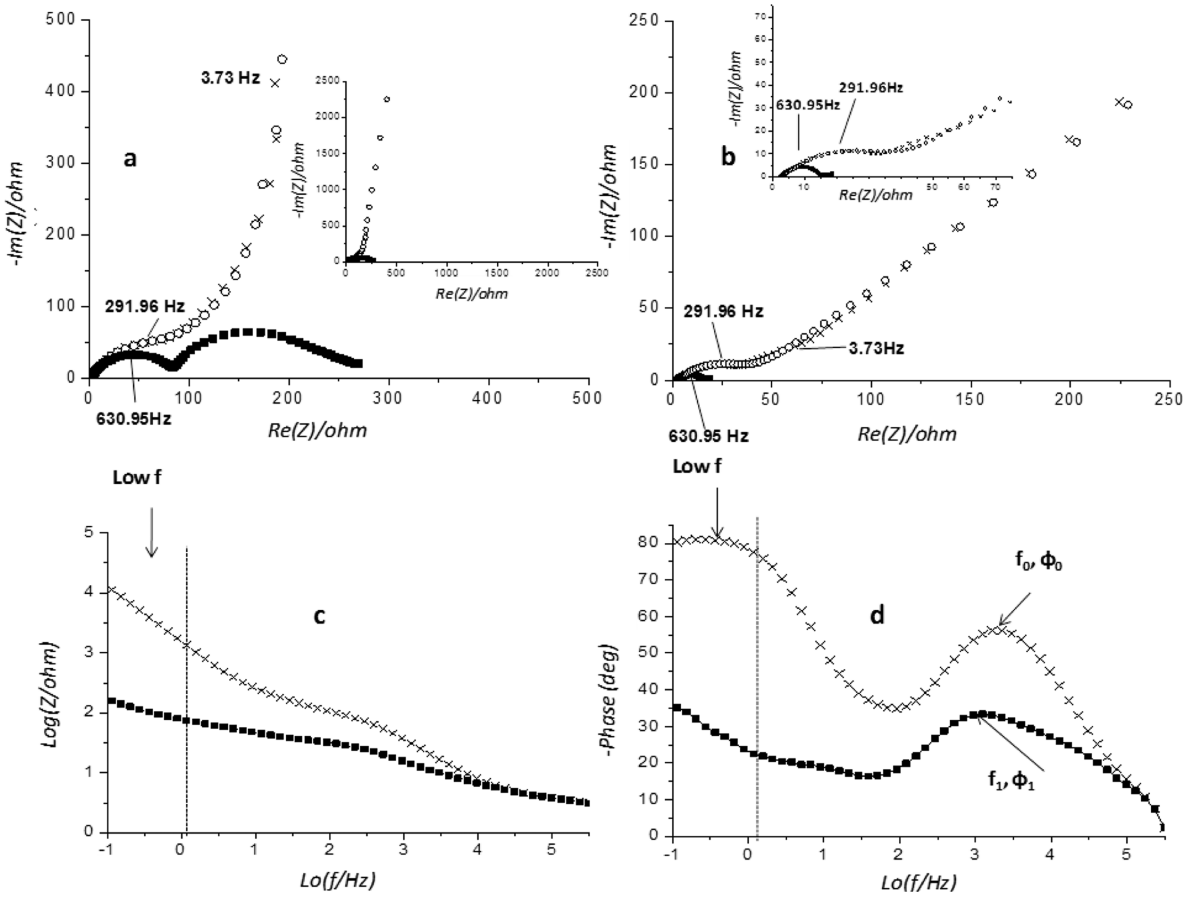

Figure 3. (a) Cole−cole representation of the impedance spectra of the Li/TiSnSb cell (open circle) and Li/Li cell (black square) at the open voltage before any polarization and (b) the same cells after polarization (one full cycle); cross symbols represent the calculated data according to the equivalent circuit of Figure 4. (c) and d) Modulus and phase angle Bode plots of Li/TiSnSb cell before (cross) and after the first charge/discharge (square).

impedance. The curve relative to the Li/TiSnSb cells exhibits at least two semicircles which merge together, one corresponding to the lithium interface at 631 Hz. At lower frequencies, the imaginary term increases rapidly with the frequency and, hence, approaches a pure capacitive behavior.

After one cycle (Figure 3b), the cell impedance decreases drastically. The semicircle at 631 Hz is clearly visible for the symmetric Li/Li cell. Looking at the IES of the Li/TiSnSb cell, it is noteworthy that the impedance of the lithium foil does not contribute significantly to the impedance excepted in a restricted high frequency domain (around 631 Hz). Hence, on the basis of the preceding result, it is stated that the depressed semicircle observed at 292 Hz before and after cell polarization is mainly due to the TiSnSb interface. At lower frequencies, the IES curve is a straight line at 45° assigned to Li diffusion through the TiSnSb electrode. This part of the IES has been modelized as a Warburg element. The depressed shape of the semicircle indicates that it includes the contribution of more than one interface and that this is characteristic of composite electrodes. The TiSnSb interface has been modelized as a serial connection of two parallel R/C (constant phase element) components and a Warburg element. The high frequency (HF) loop is the contribution of the SEI layer, and the middle frequency semicircle of the charge transfer reaction resistance in parallel with the electrochemical double layer. Contributions of electronic contact between active material and carbon conductive material or grains boundaries have not been taken into account as independent circuits. On the basis of the equivalent circuit, reported in Figure 4, the best fit for the

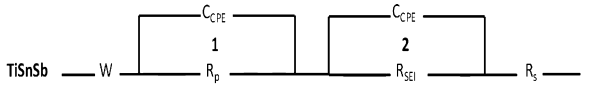

Figure 4. Scheme of the equivalent circuit corresponding to the TiSnSb interface.

different parameters have been obtained by the method of Randomize/Simplexe (Z Fit, Bio-Logic), taking account of the value of the mean square deviation χ^2. CPE (constant phase element) was used instead of ideal capacitor *C*. The fitted parameters are the solution resistance (R_s), the SEI resistance (R_{SEI}), the SEI film pseudocapacitance C_{SEI}, the double layer capacitance (C_{dl}), and finally the Warburg impedance Z_W. To reduce the number of fitting parameters and thus to decrease uncertainties in measured values, the lithium interface contribution was neglected. The starting cell (before cycling) was modeled without Warburg contribution, and Z_{SEI} was simply replaced by an interface resistance. The fitted data are summarized in Table 2.

Modulus and phase angle Bode plots are shown in Figure 3c and d. The total impedance of the cell decreases after the first charge/discharge and the formation of the SEI layer in accordance with what is seen on the curves reported in Figure 3b. In addition, before cycling the phase angle approaches 90°

dx.doi.org/10.1021/jp402973h | J. Phys. Chem. C 2013, 117, 19302−19313

Table 2. EIS Fitted Data

	before charge/discharge	after one cycle
R_s/Ω	3.9	2.4
R_p/Ω	49.3	1.4
R_{SEI}	98.9	32.9
$W/\Omega\ s^{-1/2}$		79.2
$C_{SEI}(CPE)/\mu F$	125	2.6
$C_{dl}/\mu F$	5.6	17.6

at low frequencies indicating a more capacitive behavior of the TiSnSb/electrolyte interface, and then it decreases after the discharge and SEI formation. Plots exhibit a maximum at high frequencies (at 10^3 to 2×10^3 Hz). After SEI formation, φ is lowered and the maximum is shifted to lower frequencies indicating more restricted diffusion due to the presence of the passive layer (Figure 3b, c).

In order to evaluate the effect of the cycling rate, impedance spectra were recorded at 0.5 V (hence before conversion) and for rates ranging from *C*/2 to 4*C* (Figure 5a). Before the conversion reaction, only irreversible processes related to the reduction of electrolyte components and SEI formation occur at the electrode surface. The high frequency semicircle assigned to the SEI layer decreases in diameter when the cycling rate is increased. This finding is probably linked to the thickness of the SEI layer which is assumed to be thinner and/or more conductive at high rates (4*C*) than at low rates (*C* or *C*/2). Figure 5b displays the IES of the TiSnSb electrode at different states of charge between the OCV and 0.2 V (fully lithiated state). Impedance data clearly indicate that the resistance of the SEI layer (semicircle at 291.6 Hz) increases when the potential of the electrode decreases. Such behavior may be attributed to the increase in thickness of the SEI layer at low potential due to a larger amount of reduced species accumulated at the active material surface. When the conversion reaction is completed (at 0.2 V) an additional semicircle appears at a lower frequency (up to 5 Hz) and is assigned to the internal interfaces of the converted material.

Nuclear Magnetic Resonance Spectroscopy (NMR). To investigate the chemical species formed during the cycling of TiSnSb and more specifically in the SEI, ^{7}Li ex situ NMR experiments were performed on the TSS2 cells for the first cycle. Figure 6 and Figure 7 display normalized spectra

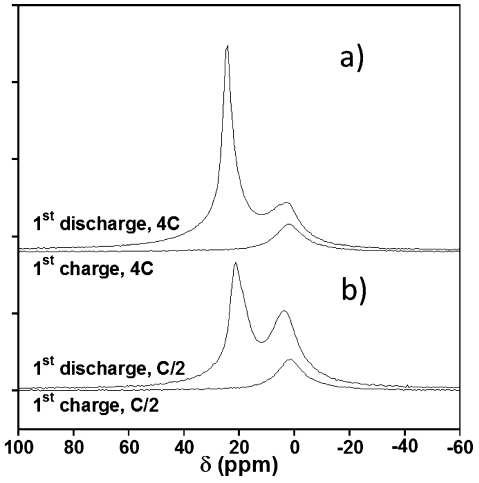

Figure 6. ^{7}Li MAS NMR spectra of the end of the first discharge and the end of the first charge of washed TiSnSb electrodes cycled at *C*/2 and 4*C*.

obtained at the end of the first discharge and at the end of the subsequent charge at *C*/2 (Figure 6a) and 4*C* rate (Figure 6b), obtained by ^{7}Li and ^{19}F NMR, respectively. The NMR spectrum of ^{7}Li at the end of a discharge at *C*/2 (Figure 6) is composed of an asymmetrical peak rising at approximately 20 ppm, along with a second peak with its maximum at 3.8 ppm. At the end of the charge, only a broad resonance centered at 2.0 ppm is observed and is assigned to diamagnetic lithiated species corresponding to the SEI.[16−18] The ^{7}Li integrated intensity measured at the end of charge corresponds to 17% of that measured at the end of discharge. A refinement of the spectrum of the end of charge shows, however, the possible presence of 4% of Li_3Sb, rising at 3.8 ppm.[19] These results are not so far from the 24% of irreversibility measured in electrochemistry, corresponding to the SEI formation, and confirm the almost

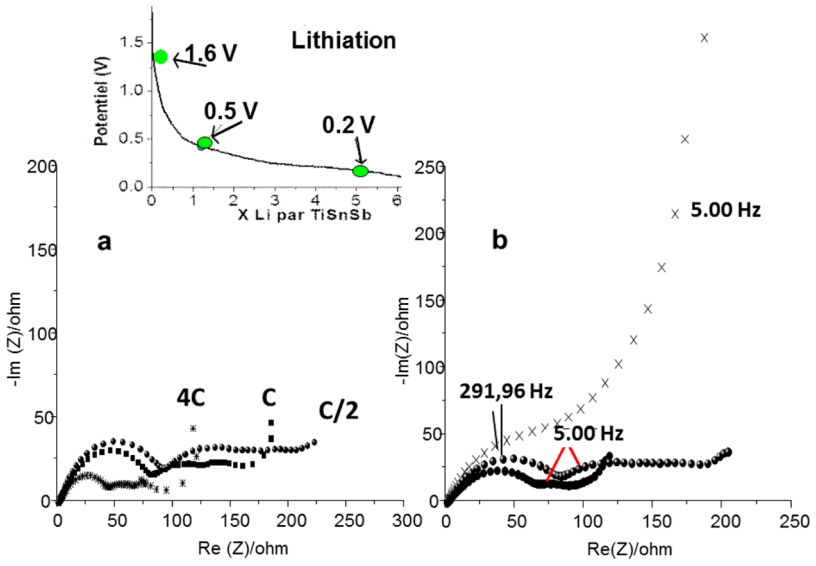

Figure 5. (a) First galvanostatic polarization of the TiSnSb electrode at 0.5 V and different rate of lithiation; (b) impedance spectra obtained at *C*/2 rate and different state of charge: 1.6 V (cross), 0.5 V (full circle), and 0.2 V (half open circle).

dx.doi.org/10.1021/jp402973h | J. Phys. Chem. C 2013, 117, 19302−19313

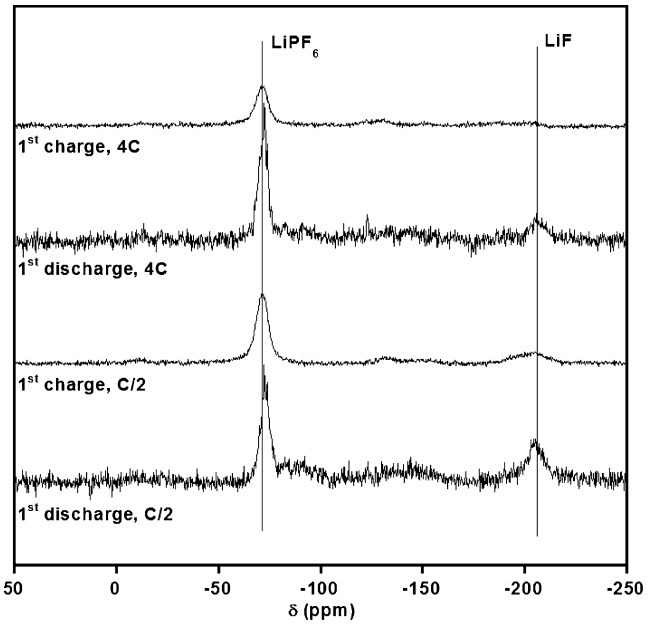

Figure 7. ^{19}F MAS NMR spectra of the end of the first discharge and the end of the first charge of washed TiSnSb electrodes cycled at *C*/2 and 4*C*.

complete reversibility of the reaction of TiSnSb conversion.[3] The presence of the signal at 2.0 ppm at the end of charge indicates also that the SEI is not completely dissolved during the charge.

A fit of the spectrum at the end of discharge has been performed, including contributions of the SEI. In addition to the resonance at 3.8 ppm, assigned to Li_3Sb, the asymmetrical peak centered at 20 ppm can be decomposed into one sharp resonance at 22 and a broader one at 19.5 ppm, assumed to correspond to either Li_xSn alloys or both Li_xSn and Li_xSb alloys. These resonances cannot be unambiguously identified since their NMR shift does not match any known values for Li_xSn alloys.[20,21] For a faster cycling rate at 4*C*, ^{7}Li NMR spectra are quite identical to those obtained at *C*/2. The sharp resonance appearing at 22 ppm on the *C*/2 sample is, however, more intensely shifted to 24 ppm for the sample cycled at 4*C*. The broader component (at 19.5 ppm for the 4*C* sample) is present and also shifted to 21 ppm. This suggests that the lithiated alloys formed at the end of discharge are slightly different in terms of composition and/or electronic properties due to the rate of lithiation used in the experiment.

^{19}F NMR spectra of the end of discharge and charge (Figure 7) show a peak at −72 ppm assigned to the electrolyte salt, indicating that the washing did not eliminate all the $LiPF_6$ traces which are certainly trapped in the porosity of the film. The presence of the $-PF_6^-$ group rather than other fluorophosphates groups such as $-PO_3F^{2-}$ or $-PO_2F_2^-$ is confirmed by the intense resonance observed at −146 ppm in ^{31}P MAS NMR. Another signal at −205 ppm is visible on the spectra, characteristic of traces of LiF. The corresponding integrated intensity is, however, lessened at the end of charge, indicating that LiF is partially dissolved upon oxidation. The presence of LiF results from the degradation of $LiPF_6$ salt described in literature due to the probable presence of water. Let us remember that CMC electrodes are prepared in water. In preliminary conclusion, a part of the SEI is dissolved at *C*/2 rate during the charge, in agreement with the solubility of several SEI lithiated species along the oxidation process, previously demonstrated by the group of Tasaki et al.[22]

^{19}F NMR spectra measured at 4*C* are again quite identical to those obtained for a *C*/2 rate. Nevertheless, the intensity of the peak at −205 ppm at the end of discharge is less important at the 4*C* rate, which shows that the amount of LiF present at the end of the discharge at this rate is smaller than that obtained at slower rate. This last point confirms the analysis by EIS and suggests an enhanced decomposition of the electrolyte salts when the electrode spends a longer time at low potentials.

The chemical shift range for diamagnetic lithium is quite narrow, and it can be difficult to discriminate among the various lithiated species present at the surface of samples coming from the real formation of SEI or from simple deposition due to electrolyte decomposition. In this purpose, the effect of washing the sample by DMC has been investigated. Figure 8a displays ^{19}F NMR spectra of nonwashed and DMC-washed electrode at the end of the first charge at *C*/2. The ^{19}F integrated intensity is divided by a factor of 45, showing the drastic effect of rinsing on the surface species. Traces of $LiPF_6$ and LiF are still observed, but all the fluorophosphates[8] have been washed away. The traces of $LiPF_6$ are assigned to unreacted electrolyte salt trapped in the porosity of the remaining SEI.

In parallel, the corresponding ^{7}Li MAS NMR spectra show a quite different evolution (Figure 8b). The ^{7}Li integrated intensity measured after washing the electrode with DMC still accounts for 70% of the intensity measured before washing. It

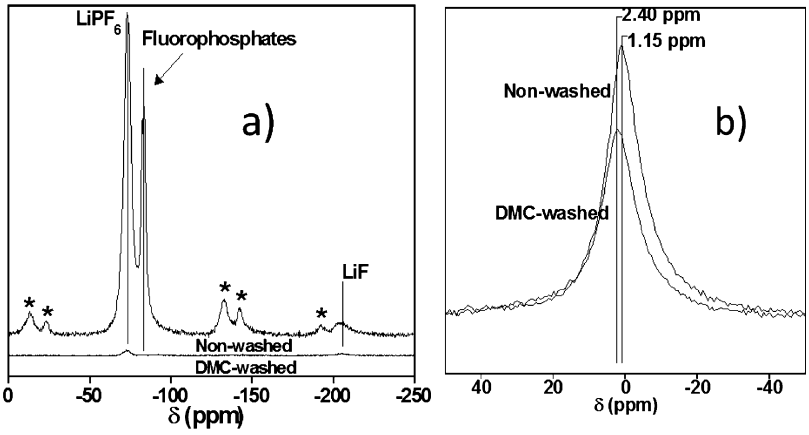

Figure 8. ^{19}F (a) and ^{7}Li (b) NMR spectra at the end of the first charge and for a nonwashed and a DMC-washed electrode.

dx.doi.org/10.1021/jp402973h | J. Phys. Chem. C 2013, 117, 19302−19313

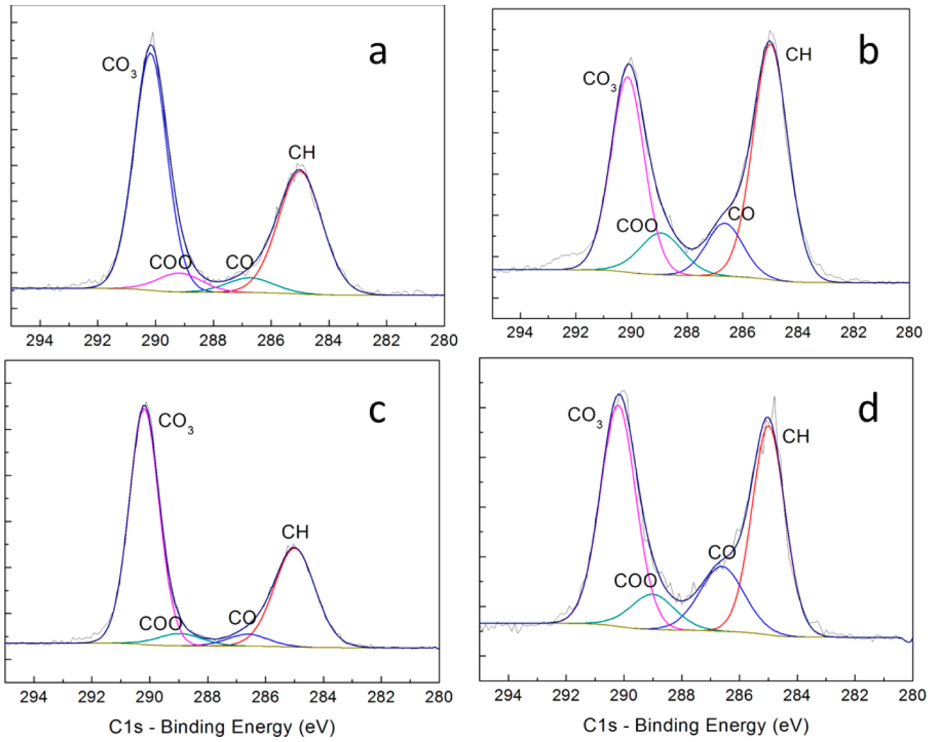

Figure 9. XPS C1s core peak spectra at (a) end of first discharge at C/2, (b) end of first charge at C/2, (c) end of first discharge at 4C, and (d) end of first charge at 4C. (* indicates the charging effect in XPS, i.e., distortion of the signal due to poor surface charge neutralization.)

Table 3. XPS Quantification Data with Corresponding Binding Energies (B.E.) and Atomic Percentages (atom %) of TiSnSb electrode after 1st Discharge/Charge at C/2 and 4C Rate, after 20th Discharge/Charge at 4C Rate

			D1-C/2-DMC	C1-C/2-DMC	D1-4C-DMC	C1-4C-DMC	D20-4C-DMC	C20-4C-DMC
		B.E. (eV)	atom %	atom %	atom %	atom %	atom %	atom %
Cls	CH	285	8.8	13.7	7.7	10.1	23.1	29.2
	CO	286.5	1.1	3.3	0.9	4.2	6.6	11.2
	COO	289	1.4	3	1	2.3	1.4	2.4
	CO_3	290.2	12.8	10.9	13.3	11.5	1.6	3.1
	SUM (%)		24.2	30.9	23	28.1	32.7	45.9
O1s	Li_2O	528.7	0.9	–	1.5	–	5.6	1.4
	Li_2CO_3 (+ LiOH)	531.9	48.2	42.8	46.8	46.8	–	–
	LiOH (+ Li_2CO_3)	531.5	–	–	–	–	28.9	24.6
		(534 eV)	–	–	–	–	–	3.6
	SUM (%)		49.1	42.8	48.3	46.8	34.5	34.4
Li 1s	Li_2O/LiOH/Li_2CO_3	55.2–55.4	26,7	23.3	28.7	24.1	30.9	17.7
	SUM (%)		26.7	23.3	28.7	24.1	30.9	17.7
F 1s	LiF	685	–	0.8	–	0.8	1.2	1.3
	$LiPF_6$	687.5	0.4	0.1	0.3	–	0.3	0.9
		(689.4 eV)	–	1.9	–	–	–	–
	SUM (%)		0.4	2.8	0.3	0.8	1.5	2.2
P2p	$P0_4$	134,134.8	–	0.1	–	–	0.36	0.5
	$LiPF_6$	136.6,137.5	–	–	–	–	<0.1	0.1
	SUM (%)		N.D.	0.1	N.D.	N.D.	0.4	0.6
Sn3d	Sn(0)3d5/2	485	–	–	–	0.02	–	–
	Sn(0) 3d3/2	493						
	SnO_x 3d5/2	487	–	0.02	–	0.07	–	–
	SnO_x 3d3/2	495						
	SUM (%)		0	0.02	0	0.1	0	0

shows that the SEI detected after washing, corresponding to species not soluble in electrolyte, is most probably composed of nonfluorinated species such as LiOH (1.5 ppm), Li_2O (2.5 ppm), Li_2CO_3 (1 ppm), and alkyl carbonates. As a matter of fact, a slight shift of the peak maximum can be also noticed from 1.1 to 2.4 ppm, indicating that signals corresponding to species removed by the washing rise at smaller chemical shifts, in agreement with smaller ^{7}Li chemical shifts expected for LiF

dx.doi.org/10.1021/jp402973h | J. Phys. Chem. C 2013, 117, 19302–19313

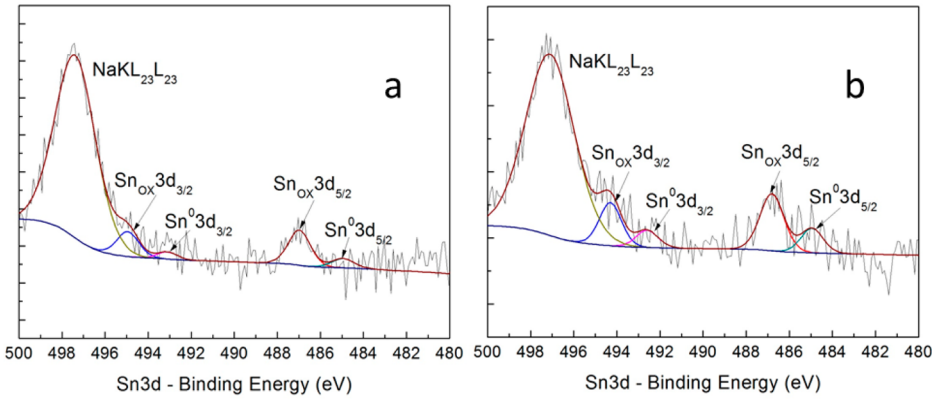

Figure 10. XPS Sn 3d core peak spectra: (a) end of first charge at C/2 and (b) end of first charge at 4C.

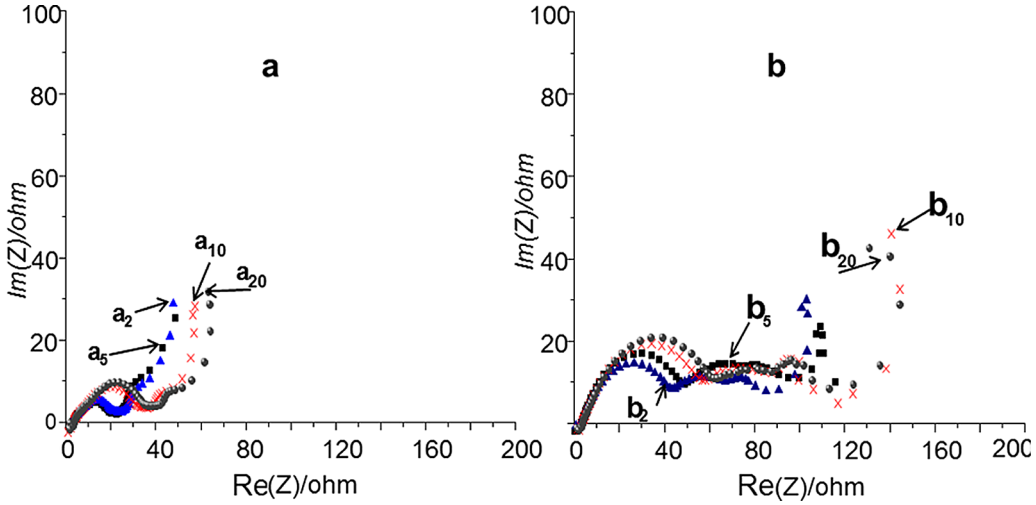

Figure 11. Nyquist plot of TiSnSb electrodes cycled at 4C rate at (a) 0.5 V and (b) 0.2 V as a function of the cycle number $a_{\text{cycle number}}$ or $b_{\text{cycle number}}$.

and $LiPF_6$, around 0 ppm. These results show in particular that the LiF and $LiPF_6$ detected by ^{19}F NMR cannot be considered as the main components of the SEI forming on TiSnSb.

X-ray Photoelectron Spectrometry (XPS). To determine the chemical species formed at the surface of the TiSnSb electrode during the cycling, XPS measurements have been performed.

Before the cycled electrodes were explored, TiSnSb electrodes were put in contact with electrolyte for 5 s, 1 h, and 24 h. No evident modification was found through XPS spectra. Therefore no significant reactivity between electrolyte and electrode could be observed without applying any current.

XPS analyses were performed on TiSnSb electrodes after first discharge/charge at different cycling rates of C/2 (Figure 9a, b) and 4C (Figure 9c, d). The results show that no signal of active material was detected in the electrode after first discharge, which reveals that no matter at which rate the electrodes were cycled, the SEI layer formed at the surface was always thicker than the depth of XPS analysis (≈5 nm).

Figure 9 presents the XPS study of C 1s core peaks. In general, all the C 1s spectra shown in the figure are quite similar; only the quantification data for each component are different, given in Table 3. Peaks located at 285.0 eV are assigned to CH_x environment, including hydrocarbon surface contamination; CO and COO bonds detected at 286.5 and 289 eV respectively are mainly contributed from organic species contained in the SEI layer and partially from alkyl carbonates, concerning its low content (1−4%) in the quantification data. The component of CO_3 detected at 290.2 eV mainly generated by Li_2CO_3, which is considered to be the major compound in SEI layer of TiSnSb electrode and also in agreement with O 1s spectra, is shown in Figure 14, where Li_2CO_3 was found at the maximum of the peak with a great proportion. Besides Li_2CO_3, CO_3 peak is partially attributed to alkyl carbonates as well. It is worth noticing that the component of CO increases and CO_3 decreases in the electrodes after first charge, which means during the charge process SEI layer partially dissolved and made it more difficult for alkyl carbonates to be detected, especially with higher cycling rate of 4C, where TiSnSb electrode shows a highest content of CO component at the surface.

Figure 10 shows the Sn 3d spectra recorded after first charge at C/2 (Figure 10a) and at 4C (Figure 10b). Peaks located at 485 and 493 eV are assigned to Sn metal; peaks at 487 and 495 eV are assigned to Sn oxide; the intense peak at 497.2 eV is given by Na $KL_{23}L_{23}$ Auger transition, which comes from CMC binder. The fact that Sn 3d peaks are observed only in the charged electrodes proves the assumption we made before: SEI layer partially dissolved during the charge process. Moreover, electrode cycled at a higher cycling rate of 4C indicates a higher content of Sn species based on the quantification data, which supports the thought given by EIS results that SEI layer is thinner in this case.

In addition, F 1s can also prove the partial dissolution of the SEI layer during charge. Indeed, salt deposition and salt

dx.doi.org/10.1021/jp402973h | J. Phys. Chem. C 2013, 117, 19302−19313

degradation products (i.e., $LiPF_6$ and LiF) should be the first layer deposited at the electrode surface. However, those compounds were covered by the SEI layer formed during the discharge process, which explains why there is only a little amount of F species (0.5% for $LiPF_6$, around 0% for LiF) detected at the end of first discharge. Then after dissolution of the SEI layer during charge, more F species were detected within the depth of XPS analysis, which results in an increase of the total amount of F species.

3.3. Aging Study. *Electrochemical Impedance Spectroscopy (EIS).* We have studied the SEI after several cycles by the same characterization techniques to better understand the aging mechanisms of the SEI upon cycling. The evolution of the SEI layer during the first cycles was investigated by impedance spectroscopy (Figure 11). A spectrum taken during the discharge at 0.5 V (beginning of conversion) (Figure 11a) and at 0.2 V (after conversion) (Figure 11b) was performed for samples at different cycle numbers. The spectra at 0.5 V (Figure 11a) showed no evolution in impedance loops during the first five cycles except at the first discharge which has been previously studied. The impedance of the cell then increases in the full frequency range. The increase of diameter of the HF and MF semicircle should indicate that the electrode/electrolyte interface is not stable and may be linked to a partial dissolution and redeposition of the SEI layer. Contrariwise, the spectra recorded after conversion (0.2 V) (Figure 11b) showed a continuous increase in size of the HF and MF semicircles reflecting an increase in the values of the SEI and charge transfer resistances. As the number of cycles increases, the thickness/resistivity of the SEI becomes more important making the displacement of ions through the SEI and the electron transfer to the active material more difficult. As the SEI is more stable at 0.5 V and is more modified from the middle of conversion reaction to the end of discharge, it is therefore suggested that the electrolyte is reduced continuously at each new created interface. As a matter of fact, Maier et al. pointed out that the middle of a conversion reaction corresponds to a phase separation and thus to the bursting of the starting material.

Let us also note that a recent study by acoustic emission performed on $NiSb_2$ showed clearly that an "earthquake" is felt by the electrode at the half of conversion.[23] As a consequence new interfaces appear in the middle of the conversion reaction that are able to catalyze the reduction of the electrolyte and increase the amount of deposits in the SEI layer. It is clear that surface films containing polymers like those obtained in the presence of VC are expected to be more cohesive and flexible and thus provide a better passivation than surface films consisting of only Li salts.[16]

Nuclear Magnetic Resonance Spectroscopy (NMR). NMR analyses have been performed to follow the evolution of the composition of the SEI in the electrode after 20 cycles. Figure 12 shows the corresponding ^{19}F NMR spectra for electrodes cycled at 4*C* and *C*/2 at the end of discharge and charge. No drastic composition change can be noticed concerning the fluorinated species. The peak at −205 ppm, corresponding to LiF, is visible on the spectra of discharge but tends to disappear at the end of charge. This partial dissolution of LiF when charging was also observed for the first cycle, confirming the cyclic process of formation and partial dissolution of LiF along the electrochemical cycling. The peak of the $LiPF_6$ is present in all spectra despite the fact that electrodes were washed with DMC probably because of the presence of $LiPF_6$ traces trapped

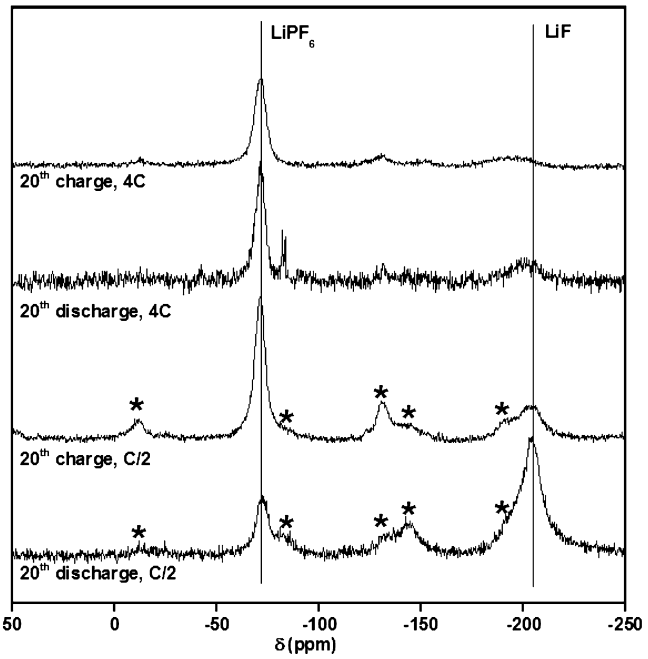

Figure 12. ^{19}F MAS NMR spectra at the end of the 20th discharge and the end of the 20th charge, for washed TiSnSb electrodes cycled at *C*/2 and 4*C* rate. Asterisks mark spinning sidebands.

within the SEI film. LiF becomes nevertheless the main fluorinated component after 20 cycles at *C*/2, a sign that the slow accumulation along the electrochemical cycling is accentuated at slower rate. It confirms that LiF formation during discharge depends on the time spent by the electrode at low potentials and is only partially compensated by dissolution or decomposition during the subsequent charge of the electrode.

The signal at −85 ppm, corresponding to fluorophosphates observed for the electrode stopped after the 20th discharge at 4*C* rate, is not observed on the other spectra and is most probably due to an incomplete cleaning.

X-ray Photoelectron Spectrometry (XPS). XPS study was also carried out on electrodes discharged/charged after 20 cycles (Figure 13a, b, respectively). Corresponding quantification data are also reported in Table 3. The first information is that the Sn 3d signal of the electrode is not observed after the 20th charge, contrary to the first charge.

This indicates an increase in thickness of the SEI layer upon cycling, which confirms the EIS results. Figure 13 indicates the C 1s core peak spectra. Compared to the first cycle, there is a significant decrease of CO_3 component located at 290.2 eV; meanwhile, the amount of CO at 286.5 eV increased, which implies that not only the thickness of the SEI layer has increased but also the composition has changed during cycling.

To further understand what happened with SEI layer, Figure 14 presents a comparison of O 1s core peak spectra recorded at 4*C* after the first (Figure 14a, b) and 20th (Figure 14c, d) cycle. The O 1s spectra recorded at the first discharge/charge show a maximum at 531.9 eV, which is in good agreement with the great proportion of Li_2CO_3. The O 1s spectra recorded after the 20th discharge/charge exhibit a slight shift toward lower binding energies, with a maximum located at 531.5 eV, in relation to the significant decrease of CO_3 component in C 1s spectra, as described above.

dx.doi.org/10.1021/jp402973h | J. Phys. Chem. C 2013, 117, 19302−19313

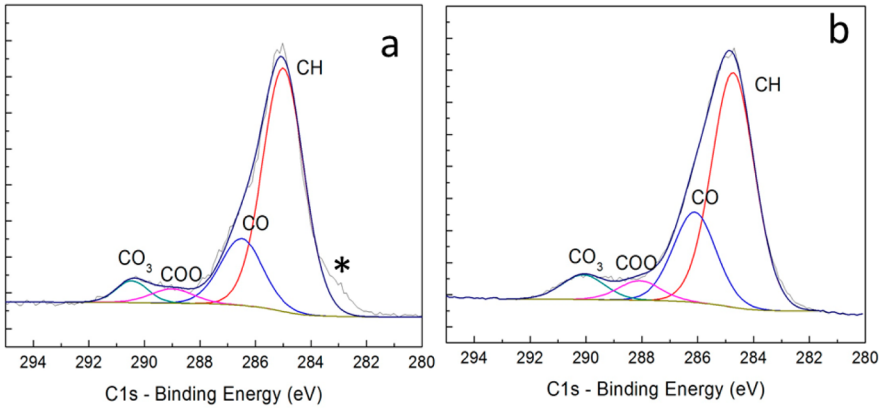

Figure 13. XPS C 1s core peak spectra at (a) end of 20th discharge at 4C and (b) end of 20th charge at 4C. (* indicates the charging effect in XPS.)

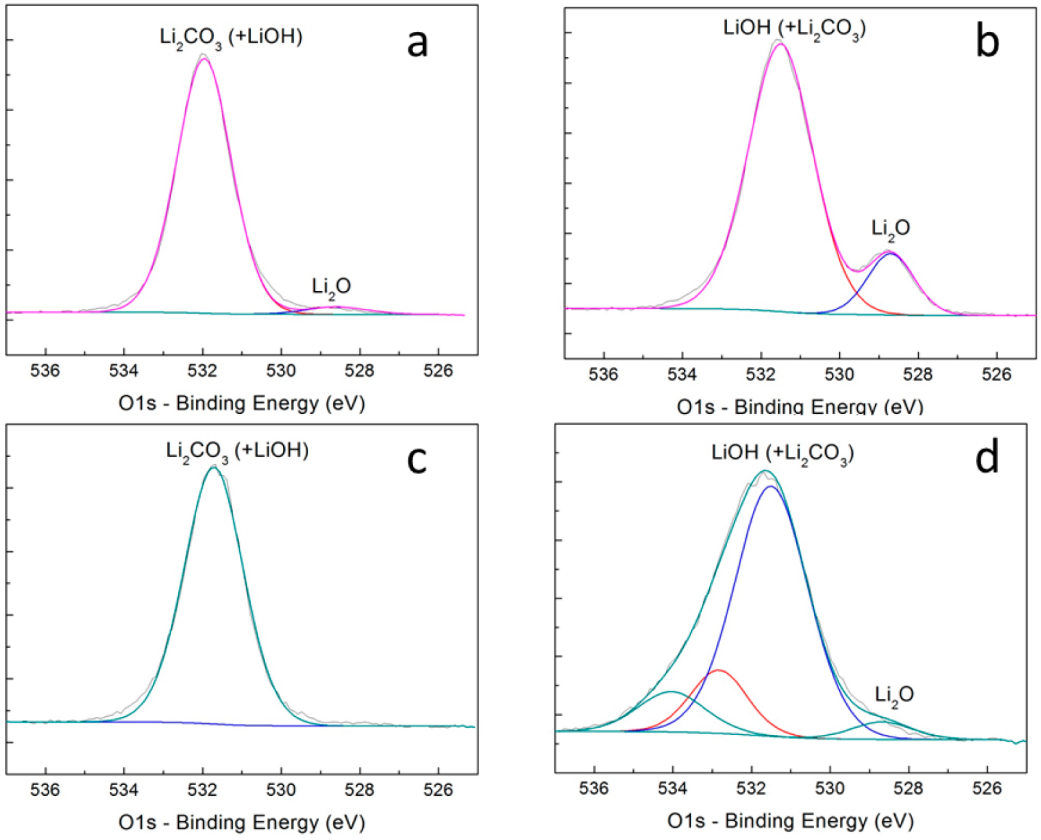

Figure 14. XPS O 1s core peak spectra at (a) end of 1st discharge at 4C, (b) end of 1st charge at 4C, (c) end of 20th discharge at 4C, and (d) end of 20th charge at 4C.

The great amount of Li species that is observed after the 20th discharge (around 31%) and 20th charge (around 18%) cannot be explained any more by Li_2CO_3, LiF, or $LiPF_6$, or other recognized species. Associated with the great amount of oxygen, it can be only attributed to the presence of LiOH at the surface. As the O 1s binding energy value of LiOH is lower than that of Li_2CO_3 (531.2 eV instead of 531.9 eV), this explains the shift observed in the spectra. Moreover, we already noticed in a previous work that LiOH may decompose into Li_2O under X-ray beam exposure inside the analysis chamber of XPS.[24] Actually this phenomenon is also observed with the present TiSnSb electrodes, as shown in Figure 14, and the Li_2O peak located at 528.7 eV was growing upon time during XPS experiment.

One of the possible explanations for the origin of LiOH is the CMC binder. Indeed, CMC binder is processed in water to prepare the electrodes, and in spite of the drying process described in the experimental section, it may retain a significant amount of water. Then the water constantly released from CMC binder generates large amounts of LiOH during cycling and changes the composition of the SEI layer.

4. CONCLUSIONS

In conclusion, at the first discharge a SEI is intensively formed at the TiSnSb electrode in alkyl carbonates containing $LiPF_6$. Reduction at 1.2 V vs Li+/Li of the VC additive is clearly visible on the CV's. The growth of the SEI continues at lower voltage until the end of the conversion reaction owing to the creation

dx.doi.org/10.1021/jp402973h | J. Phys. Chem. C 2013, 117, 19302−19313

of new interfaces. The capacity loss systematically observed during the first cycle is strongly related to that SEI growth wherein a part of Li-ions are trapped. EIS study indicates that this SEI is relatively thick and resistive, and XPS and NMR analyses prove that it is mainly constituted of lithiated carbonates species such as $ROCO_2Li$, Li_2CO_3, and probably polycarbonates but also LiF and the fluorophosphates. The compound Li_2CO_3 is the one most present upon discharge. The presence of LiOH could be related to a side reaction with the water contained in the CMC binder. During charge, a decrease in the thickness of the SEI and a reorganization of the layer caused by the contraction of the electrode occur simultaneously with partial LiF dissolution. A better Coulombic efficiency is observed when rapid cycling rates are applied. This could be related to the formation of a thinner and less resistive SEI layer at high cycling rates.

After 20 cycles a growth of the SEI is still observed, but the composition has changed with the cycle number. The major compound in SEI formed at electrode surface is no longer Li_2CO_3 but LiOH. Further analyses over longer time scalesin the future are needed for understanding the evolution of the SEI during extended cycling. This preliminary study shows that the species due to alkyl carbonate based electrolyte degradation are the same that those observed with a graphite electrode. Extended cycling tests are currently performed which should tell if the increase in SEI thickness will stop after 20− 50 cycles or if this phenomenon will continue to occur over the cycles. If this is the case, the use of more efficient SEI former additives will be required.

AUTHOR INFORMATION

Corresponding Author

*Tel.: 33 (0) 4 67 14 33 35. E-mail: Laure.monconduit@um2.fr.

Notes

The authors declare no competing financial interest.

ACKNOWLEDGMENTS

This research was performed in the framework of ALISTORE-ERI and the ANR program no. ANR-11BS09-009-01. We thank ADEME for its financial support through the Ph.D. grants of C.M and Alistore-ERI for its financial support through the Postdoc grants of H.A.W.

REFERENCES

(1) Palacin, M. R. Recent Advances in Rechargeable Battery Materials: A Chemist's Perspective. *Chem. Soc. Rev.* **2009**, *38*, 2565−2575.

(2) Cabana, J.; Monconduit, L.; Larcher, D.; Palacin, M. R. Beyond Intercalation-Based Li-Ion Batteries: The State of the Art and Challenges of Electrode Materials Reacting Through Conversion Reactions. *Adv. Mater.* **2010**, *22*, E170−E192.

(3) Sougrati, M. T.; Fullenwarth, J.; Debenedetti, A.; Fraisse, B.; Jumas, J. C.; Monconduit, L. TiSnSb, a New Efficient Negative Electrode for Li-Ion Batteries: Mechanism Investigations by Operando-XRD and Mossbauer Techniques. *J. Mater. Chem.* **2011**, *21*, 10069−10076.

(4) Wilhelm, H. A.; Marino, C.; Darwiche, A.; Monconduit, L.; Lestriez, B. Significant Electrochemical Performance Improvement of TiSnSb as Anode Material for Li-Ion Batteries with Composite Electrode Formulation and the Use of VC and FEC Electrolyte Additives. *Electrochem. Commun.* **2012**, *24*, 89−92.

(5) Jamnik, J.; Maier, J. Nanocrystallinity Effects in Lithium Battery Materials. Aspects of Nano-Ionics. *Phys. Chem. Chem. Phys. IV* **2003**, *5*, 5215−5220.

(6) Dupre, N.; Martin, J. F.; Oliveri, J.; Soudan, P.; Yamada, A.; Kanno, R.; Guyomard, D. Relationship between Surface Chemistry and Electrochemical Behavior of $LiNi_{1/2}Mn_{1/2}O_2$ Positive Electrode in a Lithium-Ion Battery. *J. Power Sources* **2011**, *196*, 4791−4800.

(7) Cuisinier, M.; Martin, J. F.; Moreau, P.; Epicier, T.; Kanno, R.; Guyomard, D.; Dupre, N. Quantitative MAS NMR Characterization of the $LiMn_{1/2}Ni_{1/2}O_2$ Electrode/Electrolyte Interphase. *Solid State Nucl. Magn. Reson.* **2012**, *42*, 51−61.

(8) Dupre, N.; Cuisinier, M.; Guyomard, D. Electrode/Electrolyte Interface Studies in Lithium Batteries Using NMR. *Electrochem. Soc. Interface (Special Issue)* **2011**, *20*, 61−67.

(9) Shirley, D. A. High-Resolution X-Ray Photoemission Spectrum of the Valence Bands of Gold. *Phys. Rev. B* **1972**, *5*, 4709−4714.

(10) Scofield, J. H. Hartree−Slater Subshell Photoionization Cross Sections at 1254 and 1487 ev. *J. Electron Spectrosc. Relat. Phenom.* **1976**, *8*, 129−137.

(11) Massiot, D.; Fayon, F.; Capron, M.; King, I.; Le Calve, S.; Alonso, B.; Durand, J. O.; Bujoli, B.; Gan, Z. H.; Hoatson, G. Modelling One- and Two-Dimensional Solid-State NMR Spectra. *Magn. Reson. Chem.* **2002**, *40*, 70−76.

(12) Zhang, X. R.; Kostecki, R.; Richardson, T. J.; Pugh, J. K.; Ross, P. N. Electrochemical and Infrared Studies of the Reduction of Organic Carbonates. *J. Electrochem. Soc.* **2001**, *148*, A1341−A1345.

(13) Fu-Ming, W.; Meng-Han, Y.; Yi-Ju Hsiao, Y. T.; Hwang, B.-J.; Wang, Y.-Y.; Wan, C.-C. Aging Effects to Solid Electrolyte Interface (SEI) Membrane Formation and the Performance Analysis of Lithium Ion Batteries. *Int. J. Electrochem. Sci.* **2011**, *6*, 1014−1026.

(14) El Ouatani, L.; Dedryvere, R.; Siret, C.; Biensan, P.; Gonbeau, D. Effect of Vinylene Carbonate Additive in Li-Ion Batteries: Comparison of $LiCoO_2/C$, $LiFePO_4/C$, and $LiCoO_2/Li_4Ti_5O_{12}$ Systems. *J. Electrochem. Soc.* **2009**, *156*, A468−A477.

(15) Aurbach, D.; Gamolsky, K.; Markovsky, B.; Gofer, Y.; Schmidt, M.; Heider, U. On the Use of Vinylene Carbonate (VC) Electrolyte Solutions for Li-Ion as an Additive to Batteries. *Electrochim. Acta* **2002**, *47*, 1423−1439.

(16) Sato, K.; Noguchi, M.; Demachi, A.; Oki, N.; Endo, M. A Mechanism of Lithium Storage in Disordered Carbons. *Science* **1994**, *264*, 556−558.

(17) Smart, M. C.; Ratnakumar, B. V.; Surampudi, S.; Wang, Y.; Zhang, X.; Greenbaum, S. G.; Hightower, A.; Ahn, C. C.; Fultz, B. Irreversible Capacities of Graphite in Lower Temperature Electrolytes for Lithium Ion Batteries. *J. Electrochem. Soc.* **1999**, *146*, 3963−3969.

(18) Meyer, B. M.; Leifer, N.; Sakamoto, S.; Greenbaum, S. G.; Grey, C. P. High Field Multinuclear NMR Investigation of the SEI Layer in Lithium Rechargeable Batteries. *Electrochem. Solid-State Lett.* **2005**, *8*, A145−A148.

(19) Monconduit, L.; Jumas, J. C.; Alcántara, R.; Tirado, J. L.; Pérez Vicente, C. Evaluation of Discharge and Cycling Properties of Skutterudite-Type $Co_{1-2y}Fe_yNi_ySb_3$ Compounds in Lithium Cells. *J. Power Sources* **2002**, *107*, 74−79.

(20) Bekaert, E.; Balaya, P.; Murugavel, S.; Maier, J.; Menetrier, M. Li-6 MAS NMR Investigation of Electrochemical Lithiation of RuO2: Evidence for an Interfacial Storage Mechanism. *Chem. Mater.* **2009**, *21*, 856−861.

(21) Marino, C.; Sougrati, M. T.; Gerke, B.; Pottgen, R.; Huo, H.; Menetrier, M.; Grey, C. P.; Monconduit, L. Role of Structure and Interfaces in the Performance of TiSnSb as an Electrode for Li-Ion Batteries. *Chem. Mater.* **2012**, *24*, 4735−4743.

(22) Tasaki, K.; Goldberg, A.; Lian, J. J.; Walker, M.; Timmons, A.; Harris, S. J. Solubility of Lithium Salts Formed on the Lithium-Ion Battery Negative Electrode Surface in Organic Solvents. *J. Electrochem. Soc.* **2009**, *156*, A1019−A1027.

(23) Villevieille, C.; Boinet, M.; Monconduit, L. Direct Evidence of Morphological Changes in Conversion Type Electrodes in Li-Ion Battery by Acoustic Emission. *Electrochem. Commun.* **2010**, *12*, 1336−1339.

(24) Dedryvere, R.; Laruelle, S.; Grugeon, S.; Poizot, P.; Gonbeau, D.; Tarascon, J. M. Contribution of X-ray Photoelectron Spectroscopy to the Study of the Electrochemical Reactivity of CoO toward Lithium. *Chem. Mater.* **2004**, *16*, 1056−1061.